

Supplementary Information

Table S1. A comparison of crystallographic parameters of Rb_2AgX_3 ($X = Br, Cl$)

Crystallographic Parameters	Rb_2AgBr_3 ¹	Rb_2AgCl_3 ²
Crystal System	Orthorhombic	Orthorhombic
Space Group	Pnma	Pnma
a (Å)	4.68	4.49
b (Å)	9.65	9.22
c (Å)	18.76	17.88
$\alpha/\beta/\gamma$ (°)	90	90

Table S2. The XPS fitting results and calculated surface atomic percentage of Rb_2AgBr_3 .

Elements	Rb		Ag		Br	
Peak binding energy (eV)	3d _{5/2}	3d _{3/2}	3d _{5/2}	3d _{3/2}	3d _{5/2}	3d _{3/2}
	109.7	111.3	368.2	374.2	68.4	69.5
Surface Atomic Percentage (%)	28.7		11.6		30.5	

Table S3. The XPS fitting results and calculated surface atomic percentages of Rb_2AgCl_3 .

Elements	Rb		Ag		Cl	
Peak binding energy (eV)	3d _{5/2}	3d _{3/2}	3d _{5/2}	3d _{3/2}	2p _{3/2}	2p _{1/2}
	109.7	111.1	368.2	374.2	198.0	199.7
Surface Atomic Percentage (%)	33.8		15.2		39.2	

Table S4. λ_{max} values from fitted PL data of Rb_2AgX_3 pellets series pressed at pressures ranging from 124.8 to 499.4 MPa against recorded powder values.

Rb_2AgX_3	PL λ_{max} / nm				
	0 MPa	124.8 MPa	249.7 MPa	374.5 MPa	499.4 MPa
Rb_2AgCl_3	585	587	589	591	594

Rb_2AgBr_3	514	502	514	514	520
--------------	-----	-----	-----	-----	-----

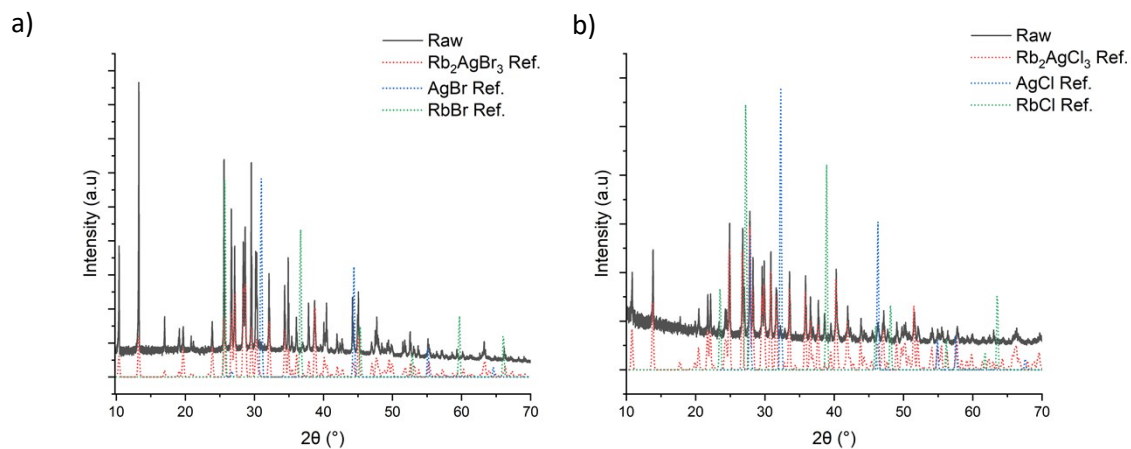


Figure S1. PXRD patterns of a) Rb_2AgBr_3 and b) Rb_2AgCl_3 as-synthesised powders compared to known references of precursor salts sourced from the ICSD database.³³

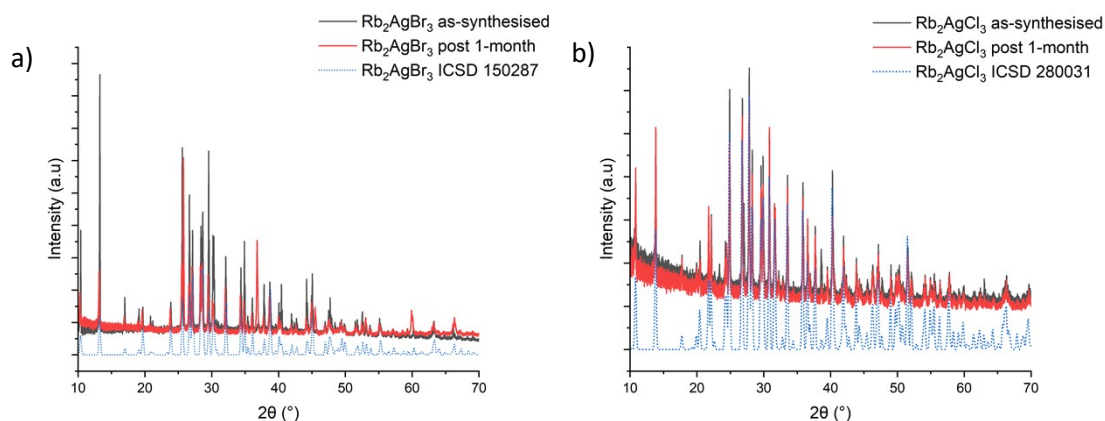


Figure S2. PXRD patterns of a) Rb_2AgBr_3 and b) Rb_2AgCl_3 depicting as-synthesised powders versus 1-month later accompanied by their respective reference patterns from the ICSD database.³³

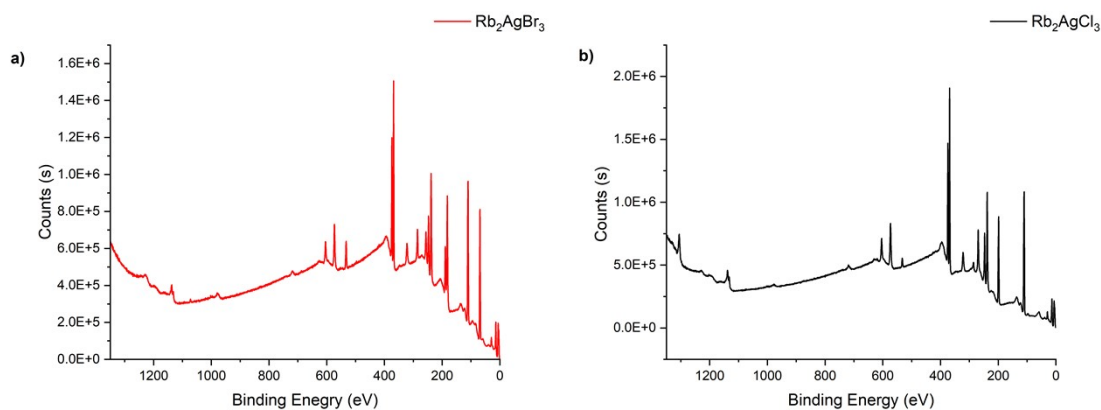


Figure S3. XPS survey spectra of a) Rb_2AgBr_3 and b) Rb_2AgCl_3

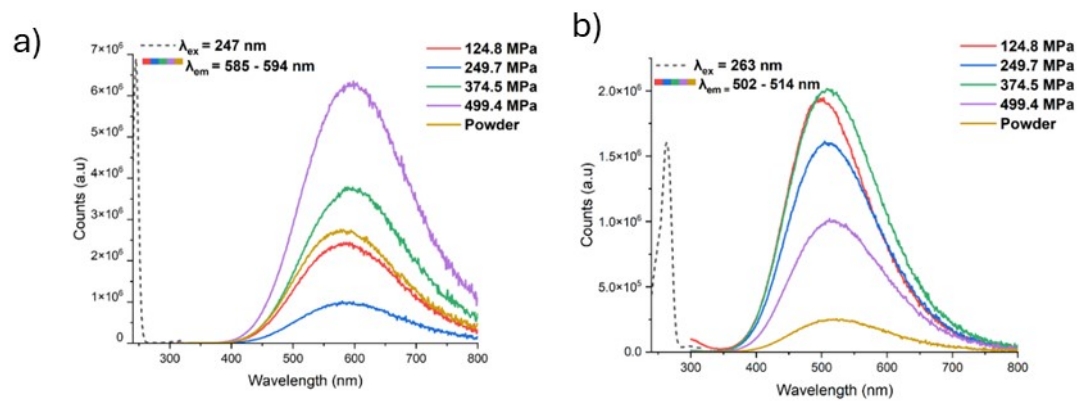


Figure S4. PL spectra of pellets of a) Rb_2AgCl_3 and of b) Rb_2AgBr_3 across pressures ranging from 124.8 to 499.4 MPa compared against PL data from powder measurements.

Thermal stability measurements of Rb_2AgX_3

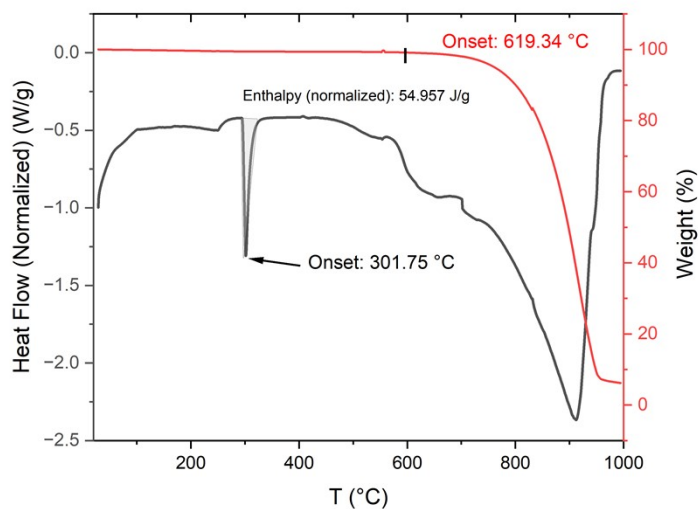


Figure S5. Thermal stability measurement of Rb_2AgCl_3 depicting thermal gravimetric analysis (TGA) data (red) overlaid with differential scanning calorimetry (DSC) data (black). Both sets of measurements were run in tandem under a N_2 flowing atmosphere from RT to 1000 °C at 10 °C/min.

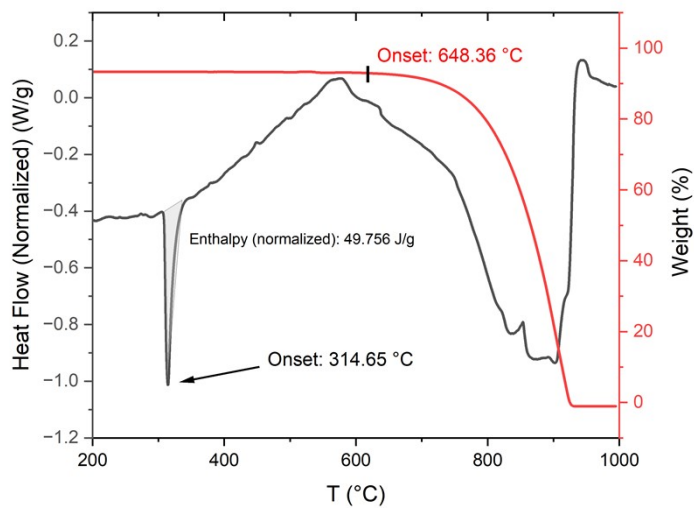


Figure S6. Thermal stability measurement of Rb_2AgBr_3 depicting thermal gravimetric analysis (TGA) data (red) overlaid with differential scanning calorimetry (DSC) data (black). Both sets of measurements were run in tandem under a N_2 flowing atmosphere from RT to 1000 °C at 10 °C/min.

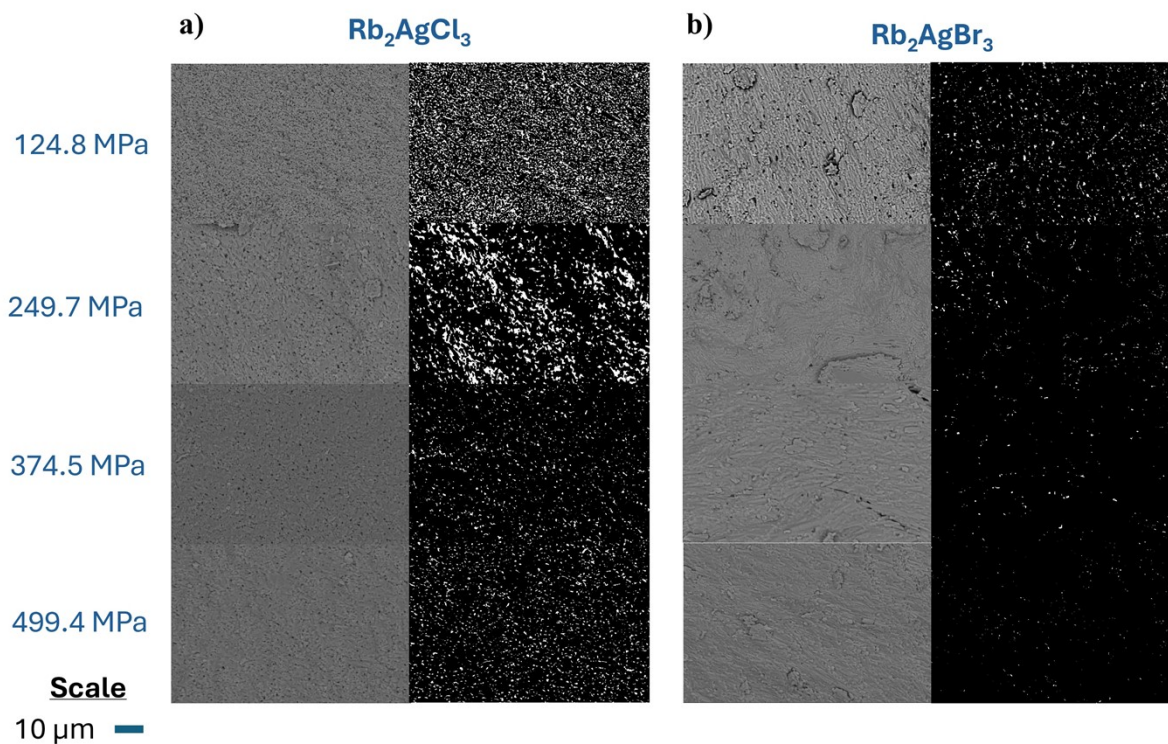


Figure S7. Cross-sectional SEM backscatter electron (BSE) images (LHS) of a) Rb_2AgCl_3 and b) Rb_2AgBr_3 10 mm \varnothing pellets illustrating the change in microstructure with increasing pressure from 124.8 MPa to 499.4 MPa. Images (RHS) rendered via ImageJTM showing pores (white) amongst the bulk of the material (black) that highlight the changes in void density with variation in pressure.

¹ S. Hull and P. Berastegui, *J Solid State Chem*, 2004, 177, 3156–3173.

² C. Hasselgren and S. Jagner, *Acta Crystallogr C*, 1999, 55, 1208–1210.